

Deep Image Feature Learning with Fuzzy Rules

Xiang Ma, Zhaohong Deng, *Senior Member, IEEE*, Peng Xu, Kup-Sze Choi, Dongrui Wu, *Senior Member, IEEE*, Shitong Wang

Abstract—Feature extraction methods are key to many image processing tasks. At present, the most popular method is to use a deep neural network, which can automatically extract robust features through end-to-end training instead of hand-crafted feature extraction. However, deep neural networks currently face some challenges: 1) their effectiveness is heavily dependent on large datasets, and 2) they are usually regarded as a black box models with poor interpretability. To meet the above challenges, a more interpretable and scalable feature learning method, deep image feature learning with fuzzy rules (DIFL-FR), is proposed in the paper, which combines a rule-based fuzzy modeling technique and a deep stacked learning strategy. The method progressively learns the image features through a layer-by-layer approach based on fuzzy rules so that the feature learning process can be better explained by the generated rules. More importantly, the learning process of the method is only based on forward propagation without back propagation and iterative learning, which results in high learning efficiency. In addition, the method is based on unsupervised learning and can be easily extended to cases of supervised and semi-supervised learning. Extensive experiments are conducted on image datasets of different scales. The results clearly show the effectiveness of the proposed method.

Index Terms—Stacked Learning; Representation Learning; TSK Fuzzy System; Image Processing

I. INTRODUCTION

IMAGE feature learning is a basic research topic in the field of computer vision and machine learning. It is very important to meet the requirements of practical applications and has been studied by many researchers in related fields. The various tasks in computer vision, such as image classification, object detection and scene segmentation, all treat feature learning as the initial step using various feature learning methods, which is followed by other techniques to achieve their goals. The design and construction of image features affect not only the task performance but also the feasibility and effectiveness of the models. In addition, it is nontrivial to design an effective method for image feature learning, since the robustness of learned features can be influenced by various factors, such as occlusion, distortion and scaling. Therefore, it is important to devise an effective method for image representation.

At present, the methods to extract image features are mainly

divided into two types: one is based on handcrafted feature extractors, and the other is based on learning through machine learning or deep learning methods.

The handcraft-based methods can extract both the global and local features. The global features usually contain all the information, including the region of interest and the background. The most representative global feature extractors are HOG [1], LBP [2], color histograms, etc. The local features can flexibly describe the internal information and details of images. A series of methods based on the bag of words [3] approach has been proposed to extract local features, such as the soft quantization [4, 5], locality-constrained linear coding [6] and, spatial pyramid [7] algorithms.

The learning-based methods can automatically obtain features without elaborately designed feature extractors. Compared with the handcraft-based methods, the learning-based methods can learn features directly from the image data and can better reveal the intrinsic information of the data. Currently, the learning-based methods are mainly based on matrix decomposition techniques and deep learning. The methods based on matrix decomposition find a mapping to transform the high-dimensional image data into low-dimensional space and utilize the potential geometric structure information of the data. Researchers assume that high-dimensional image data are actually embedded in a low-dimensional manifold in high-dimensional space. Common matrix decomposition methods include vector quantization (VQ) [8], QR decomposition [9], singular value decomposition (SVD) [10], and nonnegative matrix factorization (NMF) [11]. Turk and Pentland proposed the eigenface method [12], which applied principal component analysis (PCA) [13] to face recognition. Belhumeur et al. proposed the Fisherface [14] model, which used linear discriminant analysis (LDA) [15] to find the projection direction that maximizes the between-class scatter and minimizes the within-class scatter. The methods based on deep learning have received extensive attention in recent years. These methods extract more abstract and effective high-level information by combining the low-level features to discover different feature representations of the data [16]. Various deep learning models and structures have been proposed by researchers. Hinton et al. proposed the deep belief

This work was supported in part by the National Key Research Program of China under Grant 2016YFB0800803, the NSFC under Grant 61772239, the Jiangsu Province Outstanding Youth Fund under Grant BK20140001, the National First-Class Discipline Program of Light Industry Technology and Engineering under Grant LITE2018-02, and Basic Research Program of Jiangnan University Key Project in Social Sciences JUSRP1810ZD. (Corresponding author: Zhaohong Deng)

Xiang, Ma, Z. H. Deng, P. Xu, S. Wang are with the School of Digital Media, Jiangnan University and Jiangsu Key Laboratory of Digital Design and

Software Technology, Wuxi 214122, China (e-mail: 6171610013@stu.jiangnan.edu.cn; dengzhaohong@jiangnan.edu.cn; 6171610015@stu.jiangnan.edu.cn; wxwangst@aliyun.com)

K.S. Choi is with The Centre for Smart Health, the Hong Kong Polytechnic University (e-mail: thomask.choi@polyu.edu.hk)

D. Wu is with the Key Laboratory of the Ministry of Education for Image Processing and Intelligent Control, School of Artificial Intelligence and Automation, Huazhong University of Science and Technology, Wuhan, China (e-mail: drwu@hust.edu.cn)

network (DBN) [17], which is a generative model that can extract the high-level visual features of images. Christian et al. proposed convolutional neural networks (CNNs) [18], which have the advantages of fewer network parameters and simplified training. One key factor for the success of CNNs in image tasks is the use of convolutional architectures. To learn a filter bank in each stage of a CNN, a variety of techniques have been proposed (e.g., regularized autoencoders or their variants [19]).

The handcraft- and learning-based methods have distinctive advantages in various image processing tasks. However, they have some common defects, mainly in the following aspects: on the one hand, the handcraft-based methods tend to ignore the target object information in the image and are too sensitive to target occlusion, distortion and scaling. Furthermore, image data have some characteristics, such as huge data volume, high dimension, unstructured data shape, and uncertainty. These characteristics make handcraft-based methods not only time-consuming and laborious but also difficult to design and extract features. Hence, they cannot be directly applied to high-dimensional image analysis and processing [19]. On the other hand, the learning-based methods, such as the DNNs, have a strong hypothesis space and need to be driven by a large amount of data. When the amount of data is small, neural networks often fail to achieve satisfactory performance and easily fall into a local optimum, which leads to poor generalization ability of the model. In addition, neural networks usually need to use a back propagation [20] algorithm for training. When the number of network layers is large, the vanishing gradient problem occurs, which leads to a long training time for the model to reach convergence. In general, such a network is typically trained with the stochastic gradient descent (SGD) [21] method. However, the performance of the resulting model seriously depends on the expertise applied to parameter tuning and some ad hoc tricks. In particular, neural networks are generally considered to be black box models with poor interpretability.

To overcome the above drawbacks of the existing image feature methods, this paper proposes deep image feature learning with fuzzy rules (DIFL-FR). This method effectively combines the interpretability advantages of rule-based fuzzy systems and the layerwise feature extraction of deep learning. Specifically, the rule-based TSK fuzzy system (TSK-FS) [22–24] is first taken as a feature learning model, which is intuitive and easy to interpret. Then, the parameters of the TSK-FS are optimized by a specific feature learning objective to obtain the feature extraction model that can be interpreted by the rules. Furthermore, by means of layerwise learning, the image features are extracted layer by layer.

DIFL-FR has the following advantages. First, compared with the handcraft-based methods, DIFL-FR can automatically learn features from the data. Second, compared with a DNN, the training of DIFL-FR does not rely on large-scale data, and the results show the effectiveness on datasets with different scales. Third, DIFL-FR is based on rules and fuzzy inference to achieve feature extraction, so the process of feature extraction has better interpretability.

The main contributions of the paper are summarized as

follows:

- 1) Different from the classic TSK-FS, which is usually used for classification and regression tasks, TSK-FS is regarded as a feature extraction model for image feature extraction in this paper. Then, a novel deep image learning method based on fuzzy rules (DIFL-FR) is proposed.

- 2) By using the stacked structure and sliding window strategy of deep learning, a deep TSK-FS image feature learning method with layerwise image feature extraction capability is proposed.

- 3) Extensive experiments are conducted on image datasets with different scales. The experimental results clearly show the effectiveness and superiority of the proposed method.

The remainder of this paper is organized as follows. The related work of the proposed method is given in Section II, including the fundamentals of the convolutional neural network and TSK-FS. The details of the proposed method are illustrated in Section III. In Section IV, the experimental results and the analysis are given. Finally, the conclusions are presented in Section V.

II. RELATED WORK

The relevant knowledge of convolutional neural networks for image feature learning is reviewed first in this section. Then, the fundamentals of the TSK-FS are described briefly.

A. Convolution Neural Network

Deep learning methods are good at extracting abstract feature representations from raw data. They have hierarchical structures that include multilayer nonlinear transformations. As one of the classic deep learning models, convolutional neural networks (CNNs) [17, 25–27] have been the most widely used structures in the field of image processing. The local receptive field, shared weights and pooling in CNNs can reduce the complexity of the network. CNNs are insensitive to occlusion, distortion and scaling to some extent, which results in robustness and fault tolerance.

CNNs are mainly composed of convolutional layers, pooling layers and fully connected layers. The convolutional layer is the core of the convolutional neural network. It imitates the mechanism of the local receptive field. Convolutional operations are widely used in the field of image processing. Different convolutional kernels can extract different features, such as edges, textures or corners. In deep convolutional neural networks, different types of features, from simple to complex, can be extracted from the original image by different convolutional operations. In general, the outputs of the convolutional layer will be activated by nonlinear functions, and then, the feature maps are formed by the activated results. The commonly used activation functions include the sigmoid and the ReLU functions that have been widely used in recent years. The pooling layer, also called the subsampling layer, conducts partial downsampling on the feature maps from the previous layer. The commonly used methods include maximum pooling and average pooling. The complexity of the model can be reduced through the pooling operation, which also results in the nonsensitivity to the translation and rotation of the images. The fully connected layer is equivalent to a hidden layer in a

traditional feedforward neural network. It is usually built at the end of the CNN. The purpose of the fully connected layer is to map the features learned by the network into the label space of the samples. In some CNNs, the function of the fully connected layer can be partially replaced by global average pooling [28].

B. TSK Fuzzy System

A fuzzy system [29] is a model based on fuzzy rules and fuzzy logic. By using fuzzy sets [30] and fuzzy membership functions, a fuzzy system can directly transform human natural semantics into machine languages that can be recognized by computers. Due to their powerful learning ability and good interpretability, fuzzy systems are increasingly being applied to various fields of artificial intelligence, such as pattern recognition, intelligent control, data mining, and image processing. TSK-FS [29, 31] is one of the most popular fuzzy system models. We will explore image feature learning based on the TSK-FS in this paper, which is described as follows.

TSK-FS contains a fuzzy rule base, in which the k -th fuzzy rule can be formulated as follows:

$$\begin{aligned} R^k: & \text{ IF } x_1 \text{ is } A_1^k \wedge x_2 \text{ is } A_2^k \wedge \dots \wedge x_d \text{ is } A_d^k, \\ & \text{ THEN } f^k(\mathbf{x}) = p_0^k + p_1^k x_1 + \dots + p_d^k x_d, \end{aligned} \quad (2.1)$$

$k = 1, 2, \dots, K$

where $\mathbf{x} = [x_1, x_2, \dots, x_d]^T$ is an input vector, A_i^k is the fuzzy set [32] for the i -th feature in the k -th rule, and \wedge denotes the fuzzy conjunction operator. The final output can be calculated as follows:

$$y = \sum_{k=1}^K \frac{\mu^k(\mathbf{x})}{\sum_{k'} \mu^{k'}(\mathbf{x})} f^k(\mathbf{x}) = \sum_{k=1}^K \tilde{\mu}^k(\mathbf{x}) f^k(\mathbf{x}) \quad (2.2a)$$

where:

$$\mu^k(\mathbf{x}) = \prod_{i=1}^d \mu_{A_i^k}(x_i) \quad (2.2b)$$

$$\tilde{\mu}^k(\mathbf{x}) = \mu^k(\mathbf{x}) / \sum_{k'=1}^K \mu^{k'}(\mathbf{x}) \quad (2.2c)$$

where $\mu_{A_i^k}(x_i)$ is the membership of x_i in fuzzy set A_i^k . If multiplication is used as the conjunction operator, the firing level of the k -th rule of each sample can be formulated as (2.2b), and its normalized form is expressed in (2.2c). The Gaussian membership function is used in this paper:

$$\mu_{A_i^k}(x_i) = \exp\left(\frac{-\left(x_i - c_i^k\right)^2}{2\delta_i^k}\right) \quad (2.2d)$$

where c_i^k and δ_i^k in (2.2d) are called the antecedent parameters and can be estimated using different approaches, e.g., the fuzzy c-means clustering [33] or deterministic clustering [34] algorithms.

Once the antecedent parameters are obtained, TSK-FS can be represented as a linear model in a new feature space. The details are explained as follows. Let:

$$\mathbf{x}_e = (1, \mathbf{x}^T)^T \quad (2.3a)$$

$$\tilde{\mathbf{x}}^k = \tilde{\mu}^k(\mathbf{x}) \mathbf{x}_e \quad (2.3b)$$

$$\mathbf{x}_g = \left[(\tilde{\mathbf{x}}^1)^T, (\tilde{\mathbf{x}}^2)^T, \dots, (\tilde{\mathbf{x}}^K)^T \right]^T \quad (2.3c)$$

$$\mathbf{p}^k = (p_0^k, p_1^k, \dots, p_d^k)^T \quad (2.3d)$$

$$\mathbf{p}_g = \left[(\mathbf{p}^1)^T, (\mathbf{p}^2)^T, \dots, (\mathbf{p}^K)^T \right]^T \quad (2.3e)$$

Then, the output of TSK-FS in (2.2a) can be re-expressed as in (2.3f)

$$y = \mathbf{p}_g^T \mathbf{x}_g \quad (2.3f)$$

where $\mathbf{x}_g \in R^{K(d+1) \times 1}$ represents the feature vector in the new feature space that is transformed from the original input vector $\mathbf{x} \in R^{d \times 1}$, and \mathbf{p}_g is the combination of the consequent parameters of all the fuzzy rules.

Remark: TSK-FS has been widely used in classification and regression tasks. An interpretable discriminative model based on rules can be obtained by using labeled datasets and supervised learning methods to train the TSK-FS system. Different from the construction of classification and regression models using the classic TSK-FS, in this paper, TSK-FS is used for feature extraction tasks to implement interpretable image feature extraction based on rules.

III. DEEP IMAGE FEATURE LEARNING WITH FUZZY RULES

This section proposes DIFL-FR, a novel deep image feature learning method based on fuzzy rules. The model is a cascaded structure consisting of basic components, i.e., multilayer TSK-FS image feature learning, weight binarization, and blockwise histograms. The proposed method realizes nonlinear transformation by using the antecedent part of the multioutput TSK-FS to generate hidden features. The transformation of the hidden feature space provides a nonlinear feature learning ability similar to that of the activation functions in classic CNNs, while also having good interpretability. DIFL-FR generates different new features through multiple-group consequent parameters that are similar to the convolution kernels in CNNs. The multilayer TSK-FS image feature learning can extract deeper image features in a progressive way.

The rationale of the proposed DIFL-FR is described in five parts as follows. The overall structure of DIFL-FR is shown in Section III-A. The first and s -th layers of TSK-FS image feature learning are presented in Sections III-B and III-C, respectively. The details of the output layer are given in Section III-D.

A. The Architecture of Deep Image Feature Learning based on Fuzzy Rules

The proposed DIFL-FR is an end-to-end learning method that automatically learns features from raw data without handcraft. DIFL-FR consists of two parts, i.e., the multilayer TSK-FS image feature learning and feature output layer. The architecture of DIFL-FR with two layers of TSK-FS image feature learning is illustrated in Fig. 1.

B. The First Layer of DIFL-FR

The feature space construction is fundamental in feature learning. TSK-FS image feature learning consists of three steps:

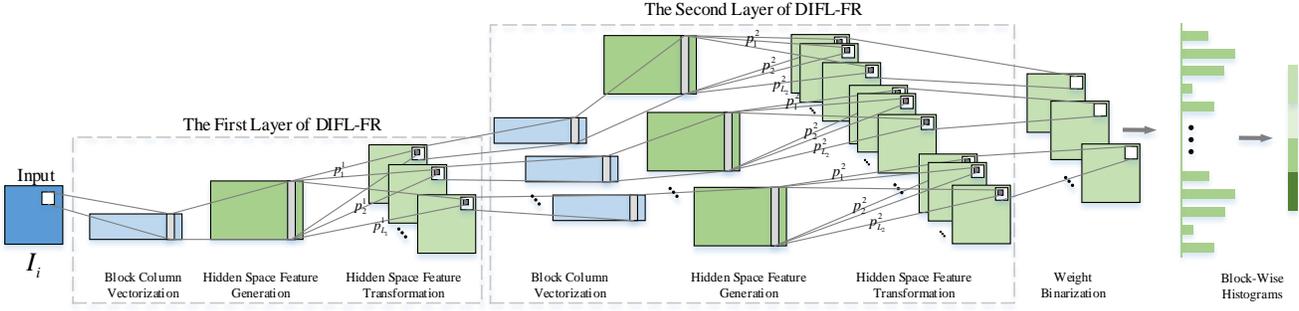


Fig. 1. The architecture of the proposed method (DIFL-FR)

the patch sliding process, feature generation in the hidden space, and feature transformation in the hidden space. Fig. S1 in Part A of the *Supplementary Martials* section shows the process of TSK-FS image feature learning. First, TSK-FS image feature learning scans the original input image and vectorizes it. Second, a nonlinear transformation is implemented by the antecedent part of the multioutput TSK-FS to generate a hidden feature space. Third, feature dimensional reduction is achieved by a linear transformation of hidden space through the consequent part of the multioutput TSK-FS. The more detailed descriptions are as follows.

Let us denote the number of input training images as N ; then, the image dataset can be represented as $\{\mathbf{I}_i\}_{i=1}^N$, and the size of each image can be represented as $m \times n$. Let the N images be concatenated as a matrix $\mathbf{I} = [\mathbf{I}_1, \mathbf{I}_2, \dots, \mathbf{I}_N]$.

1) Block Column Vectorization

For the input image I_i of size $m \times n$, considering that the spatial relationships of images have the characteristic of close local pixel connections, this paper uses a patch of size $h_1 \times h_2$ to scan each pixel of image I_i (the edges of the image are filled with 0) and then reshape each $h_1 \times h_2$ matrix into a column vector (as shown in Fig. S2 in Part A of the *Supplementary Martials* section). Then, the vector corresponding to the image I_i can be represented as (3.1).

$$\mathbf{X}_i = [\mathbf{x}_{i,1}, \mathbf{x}_{i,2}, \dots, \mathbf{x}_{i,mn}] \in R^{h_1 h_2 \times mn}, i = 1, 2, \dots, N \quad (3.1)$$

where $\mathbf{x}_{i,j} \in R^{h_1 h_2 \times 1}$ denotes the j -th vectorized patch in \mathbf{I}_i . Therefore, for all the input training images $\{\mathbf{I}_i\}_{i=1}^N$, the vector set can be represented as (3.2).

$$\mathbf{X} = [\mathbf{X}_1, \mathbf{X}_2, \dots, \mathbf{X}_N] \in R^{h_1 h_2 \times mnN} \quad (3.2)$$

2) Hidden Space Feature Generation

Based on the TSK-FS principle, the fuzzy membership in the antecedent part of the fuzzy rules can be generated according to (2.2b)-(2.2d). Fuzzy c-means (FCM) is a common method to obtain the antecedent parameters of TSK-FS, but its stability is poor due to the random initialization of FCM. Therefore, in the proposed method DIFL-FR, a deterministic clustering algorithm Var-Part is adopted to obtain the antecedent parameters. For the details of Var-Part, please see Part B of the *Supplementary Martials* section.

Once the fuzzy membership is known, according to (2.3a)-

(2.3c), the original features can be mapped from the original feature space \mathbf{X} to the hidden feature space, and the dataset \mathbf{G} of the new hidden feature space is obtained.

$$\mathbf{G} = [\mathbf{G}_1, \mathbf{G}_2, \dots, \mathbf{G}_N] \in R^{K(h_1 h_2 + 1) \times mnN} \quad (3.3a)$$

$$\begin{aligned} \mathbf{G}_i &= [\mathbf{g}_{i,1}, \mathbf{g}_{i,2}, \dots, \mathbf{g}_{i,mn}] \\ &= [\mathbf{x}_{g i,1}, \mathbf{x}_{g i,2}, \dots, \mathbf{x}_{g i,mn}] \in R^{K(h_1 h_2 + 1) \times mn} \end{aligned} \quad (3.3b)$$

$$\begin{aligned} \mathbf{g}_{i,j} &= \mathbf{x}_{g i,j} \\ &= \left[(\tilde{\mathbf{x}}_{i,j}^1)^T, (\tilde{\mathbf{x}}_{i,j}^2)^T, \dots, (\tilde{\mathbf{x}}_{i,j}^K)^T \right]^T \in R^{K(h_1 h_2 + 1) \times 1} \end{aligned} \quad (3.3c)$$

where \mathbf{G} is the concatenated data of \mathbf{G}_i for all the images in the dataset after all the images are converted into \mathbf{G}_i . \mathbf{G}_i is the matrix concatenated by $\mathbf{g}_{i,j}$ ($\mathbf{g}_{i,j} = \mathbf{x}_{g i,j}$) that is defined by (2.3a)-(2.3c). $\mathbf{g}_{i,j}$ is a vector that maps from the original feature space to the new hidden feature space through the antecedent part of the fuzzy rules, as shown in Fig. S3 in Part A of the *Supplementary Martials* section.

3) Hidden Space Feature Transformation

If the data transformed by the antecedent part of the multioutput TSK-FS is viewed as a hidden feature representation in the high-dimensional space, the consequent part of the multioutput TSK-FS can be viewed as a linear dimensional reduction of the hidden feature representation space. To preserve the geometric properties of the data during dimensional reduction, the PCA is used by maximizing the variance of the data in the hidden feature space to optimize the consequent parameters \mathbf{P} of TSK-FS. The optimization objective of the consequent parameters \mathbf{P} can be formulated as follows:

$$\max_{\mathbf{P}} \text{Tr}(\mathbf{P}^T \overline{\mathbf{G}} \overline{\mathbf{G}}^T \mathbf{P}), \text{ s.t. } \mathbf{P}^T \mathbf{P} = \mathbf{I}_{L_1} \quad (3.4a)$$

where $\overline{\mathbf{G}}$ is the matrix obtained by centralizing the hidden feature space data \mathbf{G} and \mathbf{I}_{L_1} is an identity matrix of size $L_1 \times L_1$. Specifically, for each input training image, I_i , the following centralization matrix can be obtained:

$$\overline{\mathbf{G}}_i = [\overline{\mathbf{g}}_{i,1}, \overline{\mathbf{g}}_{i,2}, \dots, \overline{\mathbf{g}}_{i,mn}] \in R^{K(h_1 h_2 + 1) \times mn} \quad (3.4b)$$

where $\overline{\mathbf{g}}_{i,j}$ is a mean-removed vector.

Thus, for all the training images $\{\mathbf{I}_i\}_{i=1}^N$, the centralization matrix of the dataset can be obtained by

$\bar{\mathbf{G}} = [\bar{\mathbf{G}}_1, \bar{\mathbf{G}}_2, \dots, \bar{\mathbf{G}}_N] \in R^{K(h_2+1) \times mnN}$. The Lagrange multiplier method is used to optimize (3.4a).

$$\bar{\mathbf{G}}\bar{\mathbf{G}}^T \mathbf{p}_g^i = \lambda_i^1 \mathbf{p}_g^i \quad (3.5a)$$

Therefore, the optimization problem in (3.4a) is transformed into the following problem of eigenvalue decomposition:

$$\mathbf{C}_1 = \mathbf{P}\Lambda_1\mathbf{P}^T \quad (3.5b)$$

with

$$\mathbf{C}_1 = \frac{1}{mnN} \bar{\mathbf{G}}\bar{\mathbf{G}}^T \in R^{K(h_2+1) \times K(h_2+1)} \quad (3.5c)$$

Λ_1 is a diagonal matrix composed of the first L_1 largest eigenvalues of \mathbf{C}_1 , i.e.,

$$\Lambda_1 = \text{diag}(\lambda_1^1, \lambda_2^1, \dots, \lambda_{L_1}^1) \quad (3.5d)$$

where $\lambda_1^1 \geq \lambda_2^1 \geq \dots \geq \lambda_{L_1}^1$. \mathbf{P} is the matrix composed of the corresponding eigenvectors as follows:

$$\mathbf{P} = [\mathbf{p}_g^1, \mathbf{p}_g^2, \dots, \mathbf{p}_g^{L_1}] \in R^{K(h_2+1) \times L_1} \quad (3.5e)$$

where $\mathbf{p}_g^{l_1}$ represents the l_1 -th eigenvector, that is, the consequent parameters corresponding to the l_1 -th output of the multioutput TSK-FS.

Once the consequent parameters \mathbf{P} are determined, the new feature data learned by TSK-FS can be obtained easily.

$$\mathbf{Z}^1 = \mathbf{P}^T \bar{\mathbf{G}} \quad (3.6a)$$

$$\mathbf{Z}^1 = [\mathbf{Z}_1^1; \mathbf{Z}_2^1; \dots; \mathbf{Z}_{L_1}^1] \quad (3.6b)$$

$$\mathbf{Z}_{l_1}^1 = [z_{i,l_1}^1, z_{i,l_1}^2, \dots, z_{i,l_1}^{mn}], \quad l_1 = 1, 2, \dots, L_1 \quad (3.6c)$$

$$z_{i,l_1}^1 = [z_{i,l_1,1}^1, z_{i,l_1,2}^1, \dots, z_{i,l_1,mn}^1], \quad i = 1, 2, \dots, N \quad (3.6d)$$

$$z_{i,l_1,j}^1 = (\mathbf{p}_g^{l_1})^T \bar{\mathbf{g}}_{i,j}, \quad i = 1, 2, \dots, N; \quad (3.6e)$$

$$l_1 = 1, 2, \dots, L_1; j = 1, 2, \dots, mn$$

Here, $z_{i,l_1,j}^1$ is the result of the j -th block in the i th image, which is obtained by the l_1 -th group of consequent parameters. It represents the features of each block. For each training image, \mathbf{I}_i , the number of results obtained by the l_1 -th group of consequent parameters is mn . These results can be reconstructed into an image of the same size as the original training image. There are L_1 groups of consequent parameters in the first layer, so that each image has L_1 new feature images. Thus, the feature image of the first layer is formed as (3.7).

$$\mathbf{I}_{i,l_1}^1 \in R^{mn \times n}, l_1 = 1, 2, \dots, L_1 \quad (3.7)$$

For all the input training images $\{\mathbf{I}_i\}_{i=1}^N$, the matrix corresponding to the set of feature images can be expressed as follows:

$$\mathbf{I}^1 = [\mathbf{I}_{1,1}^1, \mathbf{I}_{1,2}^1, \dots, \mathbf{I}_{1,L_1}^1, \dots, \mathbf{I}_{N,1}^1, \mathbf{I}_{N,2}^1, \dots, \mathbf{I}_{N,L_1}^1] \quad (3.8)$$

In addition to the PCA feature transformation criteria defined in (3.4a), other more complicated criteria can also be used to optimize the consequent parameters, \mathbf{P} . The PCA optimization criteria adopted in this paper is just a viable option.

C. The s th Layer of DIFL-FR

The process of constructing the s -th ($s \geq 2$) layer of DIFL-FR is basically the same as that of the first layer of DIFL-FR. The steps are briefly described below.

1) Block column vectorization

Refer to the steps of block column vectorization in the first layer and use the output of the $(s-1)$ -th layer for the input to the s -th layer. Similarly, for the input feature image, $\mathbf{I}_{i,\ell_{s-1}}^{s-1}$, $i = 1, 2, \dots, N$, $\ell_{s-1} = 1, 2, \dots, \Gamma_{s-1}$, $\Gamma_{s-1} = \prod_{n=s-1}^{s-1} L_{n-s}$, each pixel point has a patch of size $h_1 \times h_2$, and the information of all the points is concatenated through block vectorization to obtain (3.9).

$$\mathbf{X}_{i,\ell_{s-1}}^s = [\mathbf{x}_{i,\ell_{s-1},1}^s, \mathbf{x}_{i,\ell_{s-1},2}^s, \dots, \mathbf{x}_{i,\ell_{s-1},mn}^s] \in R^{h_2 \times mn} \quad (3.9)$$

where $\mathbf{I}_{i,\ell_{s-1}}^{s-1}$ represents the ℓ_{s-1} -th feature image of the i th original image obtained through the first $s-1$ layer TSK-FS image feature learning. $\mathbf{x}_{i,\ell_{s-1},j}^s \in R^{h_2 \times 1}$ represents the column vector of the j -th block in $\mathbf{I}_{i,\ell_{s-1}}^{s-1}$. Therefore, for each input training image \mathbf{I}_i , it can be represented as (3.10).

$$\mathbf{X}_i^s = [\mathbf{X}_{i,1}^s, \mathbf{X}_{i,2}^s, \dots, \mathbf{X}_{i,\Gamma_{s-1}}^s] \in R^{h_2 \times \Gamma_{s-1} \times mn} \quad (3.10)$$

For all the input training images $\{\mathbf{I}_i\}_{i=1}^N$, the matrix can be concatenated as (3.11).

$$\mathbf{X}^s = [\mathbf{X}_1^s, \mathbf{X}_2^s, \dots, \mathbf{X}_N^s] \in R^{h_2 \times \Gamma_{s-1} \times mnN} \quad (3.11)$$

2) Hidden Space Feature Generation

Similar to the hidden space feature generation method in the first layer of DIFL-FR, the feature matrix \mathbf{X}^s can be mapped to the new hidden feature space matrix \mathbf{G}^s that is, the new feature space spanned by the antecedent part of the rules. Then, the matrix (3.12) can be obtained. K_s represents the number of rules for the s -th layer TSK-FS image feature learning.

$$\mathbf{G}^s = [\mathbf{G}_1^s, \mathbf{G}_2^s, \dots, \mathbf{G}_N^s] \in R^{K_s(h_2+1) \times \Gamma_{s-1} \times mnN} \quad (3.12)$$

3) Hidden Space Feature Transformation

By centralizing the hidden space \mathbf{G}^s (3.13a) can be obtained as follows:

$$\bar{\mathbf{G}}^s = [\bar{\mathbf{G}}_1^s, \bar{\mathbf{G}}_2^s, \dots, \bar{\mathbf{G}}_N^s] \in R^{K_s(h_2+1) \times \Gamma_{s-1} \times mnN}, \quad (3.13a)$$

$$\Gamma_{s-1} = \prod_{n=s-1}^{s-1} L_{n-s}$$

$$\bar{\mathbf{G}}_i^s = [\bar{\mathbf{g}}_{i,1}^s, \bar{\mathbf{g}}_{i,2}^s, \dots, \bar{\mathbf{g}}_{i,\Gamma_{s-1}}^s] \in R^{K_s(h_2+1) \times \Gamma_{s-1} \times mn}, \quad (3.13b)$$

$$i = 1, 2, \dots, N$$

$$\bar{\mathbf{g}}_{i,\ell_{s-1}}^s = [\bar{\mathbf{g}}_{i,\ell_{s-1},1}^s, \bar{\mathbf{g}}_{i,\ell_{s-1},2}^s, \dots, \bar{\mathbf{g}}_{i,\ell_{s-1},mn}^s] \in R^{K_s(h_2+1) \times mn}, \quad (3.13c)$$

$$\ell_{s-1} = 1, 2, \dots, \Gamma_{s-1}$$

where $\bar{\mathbf{g}}_{i,\ell_{s-1},j}^s$ is a mean-removed vector.

As with the first layer of DIFL-FR, the PCA optimization criterion is used to solve for the consequent parameters $\mathbf{P}^s = [\mathbf{p}_g^{s,1}, \mathbf{p}_g^{s,2}, \dots, \mathbf{p}_g^{s,L_s}] \in R^{K_s(h_2+1) \times L_s}$ of the s -th layer of DIFL-FR. Here, \mathbf{p}_g^{s,l_s} represents the consequent parameter

corresponding to the l_s -th output of the multioutput TSK-FS.

Once the consequent parameters, \mathbf{P}^s , are determined, the new feature learned by the s -th layer of DIFL-FR can be obtained:

$$\mathbf{Z}^s = (\mathbf{P}^s)^\top \overline{\mathbf{G}}^s \quad (3.14a)$$

$$\mathbf{Z}^s = [\mathbf{Z}_1^s; \mathbf{Z}_2^s; \dots; \mathbf{Z}_{L_s}^s] \quad (3.14b)$$

$$\mathbf{Z}_{l_s}^s = [\mathbf{Z}_{1,l_s}^s, \mathbf{Z}_{2,l_s}^s, \dots, \mathbf{Z}_{N,l_s}^s], \quad l_s = 1, 2, \dots, L_s \quad (3.14c)$$

$$\mathbf{Z}_{i,l_s}^s = [\mathbf{z}_{i,l_s,1}^s, \mathbf{z}_{i,l_s,2}^s, \dots, \mathbf{z}_{i,l_s,\Gamma_{s-1}}^s], \quad (3.14d)$$

$$i = 1, 2, \dots, N, \quad \Gamma_{s-1} = \prod_{n=s-1}^{s-1} L_{n-s}$$

$$\mathbf{z}_{i,l_s,\ell_{s-1}}^s = [\mathbf{z}_{i,l_s,\ell_{s-1},1}^s, \mathbf{z}_{i,l_s,\ell_{s-1},2}^s, \dots, \mathbf{z}_{i,l_s,\ell_{s-1},mn}^s], \quad (3.14e)$$

$$\ell_{s-1} = 1, 2, \dots, \Gamma_{s-1}$$

$$\mathbf{z}_{i,l_s,\ell_{s-1},j}^s = (\mathbf{p}_{j,l_s}^{s,l_s})^\top \mathbf{g}_{i,\ell_{s-1},j}^s, \quad j = 1, 2, \dots, mn \quad (3.14f)$$

where $\mathbf{z}_{i,l_s,\ell_{s-1},j}^s$ represents the new feature of the j -th block in the ℓ_{s-1} -th feature image $\mathbf{I}_{i,\ell_{s-1}}^{s-1}$, which is obtained by the l_s -th group of consequent parameters of the s -th layer TSK-FS. $\mathbf{I}_{i,\ell_{s-1}}^{s-1}$ represents the ℓ_{s-1} -th feature image obtained after the i th original image is learned by the first $s-1$ layer TSK-FS image feature learning. For each input feature image, $\mathbf{I}_{i,\ell_{s-1}}^{s-1}$, a total of mn new feature values, $\mathbf{z}_{i,l_s,\ell_{s-1},j}^s$, can be obtained. These results can be reconstructed into an image of the same size as the original training image. Thus, the feature image, $\mathbf{I}_{i,l_s,\ell_{s-1}}^s$, is formed. There are L_s groups of consequent parameters in the s -th layer, so that each input feature image, $\mathbf{I}_{i,l_s,\ell_{s-1}}^s$, can generate L_s new feature images $\{\mathbf{I}_{i,l_s,\ell_{s-1}}^s, l_s = 1, 2, \dots, L_s\}$. For each original image, a total of $\Gamma_s (\Gamma_s = \prod_{n=s-1}^s L_{n-s})$ feature images can be obtained. Therefore, for all the input training images, $\{\mathbf{I}_i\}_{i=1}^N$, after s -layer TSK-FS image feature learning, the feature image set can be represented as follows:

$$\{\mathbf{I}_{i,l_s}^s \in R^{m \times n}\}, \quad i = 1, 2, \dots, N; \ell_s = 1, 2, \dots, \Gamma_s; \Gamma_s = \prod_{n=s-1}^s L_{n-s}$$

The above feature image set, \mathbf{I}^s , can be represented as the following matrix form:

$$\mathbf{I}^s = [\mathbf{I}_{1,1}^s, \mathbf{I}_{1,2}^s, \dots, \mathbf{I}_{1,\Gamma_s}^s, \dots, \mathbf{I}_{N,1}^s, \mathbf{I}_{N,2}^s, \dots, \mathbf{I}_{N,\Gamma_s}^s], \quad (3.15)$$

$$\Gamma_s = \prod_{n=s-1}^s L_{n-s}$$

D. The Output Layer

The output layer of DIFL-FR first performs weight binarization on the feature image extracted by the previous multiple cascaded TSK-FSs and then converts it into a block histogram statistical vector as the final feature extracted by the model.

1) Weight Binarization

The output layer first binarizes the feature image obtained by the s -th layer; the binarization function is defined as follows:

$$\mathbf{P}_{i,l_s,\ell_{s-1}} = H(\mathbf{I}_{i,l_s,\ell_{s-1}}^s), \quad i = 1, 2, \dots, N; \quad (3.16)$$

$$l_s = 1, 2, \dots, L_s; \ell_{s-1} = 1, 2, \dots, \Gamma_{s-1}$$

where $H(x) = \begin{cases} 1, & x \geq 0 \\ 0, & x < 0 \end{cases}$ is a Heaviside step function.

For the L_s binary images generated by the ℓ_{s-1} -th feature image, the value of each pixel at the same position is regarded as one of the L_s -bit binary numbers. Thus, these L_s binary images can be converted into an integer-valued feature image, which is denoted as $\mathbf{T}_{i,\ell_{s-1}}$. $\mathbf{T}_{i,\ell_{s-1}}$ represents an integer-valued feature image generated by the ℓ_{s-1} -th feature image, which is obtained from the i th original input image in the s -th layer. Every pixel in $\mathbf{T}_{i,\ell_{s-1}}$ is an integer in the range $[0, 2^{L_s} - 1]$.

$$\mathbf{T}_{i,\ell_{s-1}} = \sum_{l_s=1}^{L_s} 2^{l_s-1} \mathbf{P}_{i,l_s,\ell_{s-1}} \quad (3.17)$$

All the integer-valued feature images corresponding to all the training images can be expressed as the following matrix:

$$\mathbf{T} = [\mathbf{T}_{1,1}, \mathbf{T}_{1,2}, \dots, \mathbf{T}_{1,\Gamma_{s-1}}, \dots, \mathbf{T}_{N,1}, \mathbf{T}_{N,2}, \dots, \mathbf{T}_{N,\Gamma_{s-1}}].$$

2) Blockwise Histograms

This paper uses a block of size $h_1 \times h_2$ to slide the integer-valued feature image $\mathbf{T}_{i,\ell_{s-1}}$ with overlap ratio of Cr (the default value is 0.5, that is, the step size is $\lfloor h_1 / 2 \rfloor, \lfloor h_2 / 2 \rfloor$) and partition, $\mathbf{T}_{i,\ell_{s-1}}$, into B blocks. For each block, the histogram (in the range $[0, 2^{L_s} - 1]$) of the decimal values can be computed, and the output of each block is a 2^{L_s} -dimensional vector. For $\mathbf{T}_{i,\ell_{s-1}}$, there is a total of B blocks, and these 2^{L_s} -dimensional vectors can be concatenated into a vector, expressed as $\mathbf{h}_{i,\ell_{s-1}} = \text{Hist}(\mathbf{T}_{i,\ell_{s-1}}) \in R^{(2^{L_s})^{\Gamma_{s-1} \times 1}}$, where $\text{Hist}(\cdot)$ is the operator that uses the block histogram statistics and expands the result as a vector.

For an original input image, after k -layer image feature learning based on TSK-FS, weight binarization and blockwise histogram operations, the output feature vector can be expressed as

$$\mathbf{f}_i = [\mathbf{h}_{i,1}, \mathbf{h}_{i,2}, \dots, \mathbf{h}_{i,\Gamma_{s-1}}] \in R^{(2^{L_s})^{\Gamma_{s-1} \times B \times 1}}, \quad (3.18)$$

$$\Gamma_{s-1} = \prod_{n=s-1}^s L_{n-s}$$

Therefore, the original image dataset, $\{\mathbf{I}_i\}_{i=1}^N$, can be transformed into the feature matrix (3.19).

$$\mathbf{F} = [\mathbf{f}_1, \mathbf{f}_2, \dots, \mathbf{f}_N] \in R^{(2^{L_s})^{\Gamma_{s-1} \times B \times N}}, \Gamma_{s-1} = \prod_{n=s-1}^{s-1} L_{n-s} \quad (3.19)$$

Finally, the extracted features can be put into a common classifier for learning.

For the details of the multioutput TSK-FS, please see Part C of the *Supplementary Materials* section. Table S1 in part D of the *Supplementary Materials* section provides a detailed algorithm description of the proposed DIFL-FR method.

IV. EXPERIMENTS

Extensive experiments are conducted to evaluate the effectiveness of the proposed image extraction method DIFL-FR. Specifically, the performance of the proposed method on small-scale and larger-scale image datasets is discussed. In this section, DIFL-FR with two layers is selected for the experiments. If there is no specific description of the layers, DIFL-FR with two layers is selected for the experiments in this section.

To evaluate the classification performance, a classifier is required that is trained based on the extracted image features, and then the classification accuracy is used as the indicator to evaluate the performance. In our experiments, the multiclass linear SVM [35] is selected as the classifier.

A. Small-Scale Datasets

In this section, the proposed method DIFL-FR is evaluated on two small-scale face recognition datasets [36–38], the ORL and Extended Yale B datasets.

In the experiments, two handcraft-based methods and three learning-based methods with matrix decomposition are used as the comparative algorithms. Due to the small size of the adopted datasets, the DNNs perform poorly on them, and therefore the algorithms based on DNNs are not included for comparison in this section. Meanwhile, the original images are treated as outputs of the benchmark algorithm (represented as Raw), where the original pixels of the image are directly used for the classifier without feature extraction. The two handcraft-based methods are the block histogram (BlockHist) and local binary pattern (LBP) methods. The three learning-based methods are the principal component analysis (PCA), kernel principal component analysis (KPCA) and Fisherface method.

The five-fold cross-validation approach is adopted to search for the optimal parameter settings for all the comparative algorithms, and the maximum mean accuracy is reported.

For the BlockHist method, the overlap ratio, Cr , is set as 0.5, and the block size is optimally set by searching grid $h=\{3,5,7,9,11\}$. For LBP, the image is equally divided into 4×4 subareas. In each subarea, the histogram is counted using the uniform LBP, and then the obtained statistical histogram of each subarea is concatenated as one feature vector. For the PCA and KPCA, the dimension of the subspace is optimally set by searching grid $m=\{10,12,14,\dots,400\}$. The Gaussian kernel is used for the KPCA, and the parameters of the Gaussian kernel are optimally set by searching grid $t=\{2^{-4},2^{-3},\dots,2^4\}$. For the Fisherface method, the dimension of the subspace is fixed to the number of categories -1.

For the proposed method DIFL-FR, the block size of each pixel is set as 5×5 , and the overlap ratio Cr in the output layer is set as 0.5. For DIFL-FR with two layers of TSK-FS, the two important parameters are the number of rules for each layer and the number of groups for calculating the consequent parameters in each feature learning phase. They are optimally set by searching grids $K_1, K_2 = \{2, 3, \dots, 10\}$ and

$$L_1, L_2 = \{4, 5, \dots, 16\}.$$

To comprehensively verify that DIFL-FR can achieve good performance when the amount of training data is small, the training set and test set are divided into different proportions, and the details of the datasets are shown in Part E of the *Supplementary Materials* section

1) ORL Dataset

The ORL face dataset consists of 400 face images taken by the AT&T Lab from April 1992 to April 1994, with a total of 40 distinct subjects. All the images were taken at different times, with varying lighting, different facial expressions (open / closed eyes, smiling / not smiling) and different facial details (glasses / no glasses). For each subject, 10 images were taken in an upright, frontal position (with tolerance for some side movement). The ORL dataset is the most widely used benchmark face dataset. In this section, the size of each image is resized to 32×32 pixels, with 256 gray levels. Table I shows the classification results of different methods on the ORL dataset with different proportions of the training set and test set.

To verify whether the DIFL-FR has good robustness to noise, we added some typical types of noise (e.g., salt & pepper noise and Gaussian noise) in the training set and test set of ORL_Train_8 (see Fig. 2). The experimental classification results are shown in Table II, which shows that DIFL-FR is more robust to noise than the comparative methods.

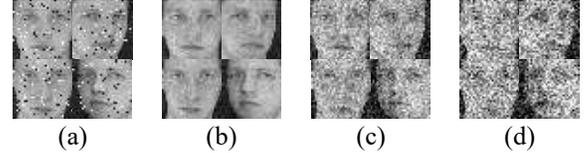


Fig. 2. ORL Samples with noise: (a) salt & pepper noise, (b) 10std Gaussian noise, (c) 30std Gaussian noise, (d) 50std Gaussian noise; 10std Gaussian represents that in ORL_Train_8, Gaussian noise with 10 standard deviations is added to the training set and test set.

To explore whether DIFL-FR is robust to occlusion, this section uses the same training set as in ORL_Train_8 but a different test set, where an unrelated image is used to replace a randomly located region of an image to simulate various levels of contiguous occlusion from 20% to 60% (some images are shown in Fig. 3). It can be seen from the experimental results in Table III that DIFL-FR is superior to the other comparison algorithms under different levels of occlusion. With 20% of pixels occluded, DIFL-FR achieves an astonishing 99.75% accuracy and still maintains an accuracy of 82.25% even when the occlusion level increases to 60%. It can be concluded that not only is DIFL-FR noise-insensitive, but it also has strong robustness to occlusion.

2) Extended Yale B Dataset

The extended Yale B dataset consists of 2414 images of 38 individuals. For each individual, approximately 64 near frontal

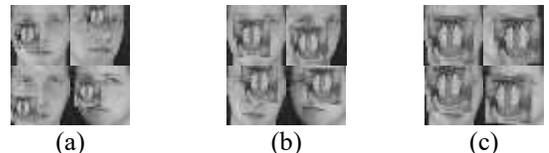


Fig. 3. Test face image with various levels of occlusion on the ORL dataset: (a)20% Occlusion. (b)40% Occlusion. (c)80% Occlusion.

TABLE I
COMPARISON OF THE ACCURACY ON ORL DATASET WITH DIFFERENT PROPORTIONS OF TRAINING SET AND TEST SET FOR EACH METHOD (%)

Method	DIFL-FR	Raw	BlockHist	LBP	PCA	KPCA	Fisherface
ORL_Train_2	89.44±2.35	82.5±0.96	70.44±1.93	82.31±1.95	81.75±0.81	81.56±1.96	79.75±1.58
ORL_Train_5	97.7±1.04	94.3±0.76	87.2±1.82	93.9±1.56	94.1±1.08	92.7±1.15	92.9±1.14
ORL_Train_8	99.5±0.68	98±1.9	96.75±1.9	98.25±1.43	98.25±1.68	98±1.9	96.25±1.98

TABLE II
COMPARISON OF THE ACCURACY ON THE ORL_TRAIN_8 DATASET WITH DIFFERENT NOISES FOR EACH METHOD (%)

Method	DIFL-FR	Raw	BlockHist	LBP	PCA	KPCA	Fisherface
Salt & pepper	98.5±1.37	92.75±1.63	96.75±2.44	95.75±2.59	90.25±1.05	96.75±1.43	86.25±2.34
10 std gaussian*	99.75±0.56	98.25±1.68	88.25±4.29	81±2.24	98±1.9	98±1.9	95.25±1.05
30 std gaussian	99±3.85	94.75±2.4	56.75±2.59	19.75±4.45	94.25±2.44	96.75±1.9	88±2.27
50 std gaussian	93.75±3.85	83±3.6	51±5.69	5.5±4.73	79.75±4.09	91±3.35	70.75±3.6

*: 10std Gaussian represents that in ORL_Train_8, the Gaussian noise with 10 standard deviation is added to the training set and test set.

TABLE III
COMPARISON OF ACCURACY ON THE ORL_TRAIN_8 DATASET WITH VARYING LEVELS OF OCCLUSION IN THE TEST SET FOR EACH METHOD (%)

Method	DIFL-FR	Raw	BlockHist	LBP	PCA	KPCA	Fisherface
20% Occlusion	99.75±0.56	91.25±1.77	95±3.42	97±2.59	90.5±2.09	94±1.05	81.75±2.88
40% Occlusion	98.25±2.09	55.75±4.56	86.5±4.37	80.5±1.12	53±5.2	65±4.92	41.75±2.09
60% Occlusion	82.25±6.27	14.25±3.14	74.75±4.63	34.75±1.63	15.25±3.89	29.5±2.88	13±3.81

TABLE IV
COMPARISON OF ACCURACY ON EYALEB DATASET WITH DIFFERENT PROPORTIONS OF TRAINING SET AND TEST SET FOR EACH METHOD (%)

Method	DIFL-FR	Raw	BlockHist	LBP	PCA	KPCA	Fisherface
EYaleB_Train_10	84.27±1.41	81.97±2.37	43.9±0.81	80.23±0.89	81.97±2.39	71.73±1.59	83.59±1.32
EYaleB_Train_30	99.12±0.22	95.59±0.61	71.59±0.91	95.86±0.39	95.54±0.64	90.63±1.12	81.27±1.23
EYaleB_Train_50	99.46±0.16	98.44±0.36	79.53±0.87	97.82±0.16	98.48±0.52	94.59±0.1	97.59±0.56

images were taken under different illumination conditions. In this section, the size of each image is resized to 32×32 pixels, with 256 gray levels.

The experimental results are shown in Table IV. The classification accuracy of DIFL-FR is superior to that of the other comparative algorithms. On the EYaleB_Train_50 dataset, the DIFL-FR achieves 99.46% accuracy, and it can be concluded that DIFL-FR has strong robustness to illumination.

B. Larger-Scale Datasets

In this section, the proposed method DIFL-FR is evaluated on larger-scale datasets. Specifically, the experiments are conducted on the MNIST [25] and Fashion-MNIST [39] datasets.

1) MNIST Dataset

In this section, the MNIST dataset, which is a handwritten digital set created by the AT&T Lab, is used for experiments. It contains 60,000 training images and 10,000 test images. The dataset is composed of handwritten digit (0 to 9) images. All the digit images were size-normalized to 28×28 pixels, with 256 gray levels.

To effectively evaluate the performance of the proposed method DIFL-FR, in addition to using the same comparative methods on small-scale datasets, some DNNs are also included. This section first evaluates a very simple CNN (6-2-16-2) structure that consists of two convolutional layers, two pooling layers and two fully connected layers. Each convolutional layer has 6 and 12 convolutional kernels of size 5×5 . The mean square error is selected as the loss function, and the sigmoid function is selected as the activation function. The SGD

algorithm is used to optimize the network, and the number of training epochs is set as 100. This section also compares a classic CNN structure, LeNet-5, and a generative model DBM [40]. The DBM is a Boltzmann machine with multiple hidden layers. Since DIFL-FR is an unsupervised deep feature learning method, we also select an unsupervised deep network, StrongNet [41], for comparison. StrongNet is an unsupervised backpropagation-free architecture with three-layers, and its tail layer is trained using a simple linear classifier. Table V shows the classification accuracies of these methods on the MNIST dataset. Of these methods, the proposed method DIFL-FR performs best.

The MNIST homepage (<http://yann.lecun.com/exdb/mnist/>) includes both the dataset itself and an extensive list of results achieved with different methods. Since this paper evaluates a DIFL-FR with two-layer image feature learning and an output layer, its performance is compared with the two/three-layer models. The classification errors of the fourteen different two/three-layer neural networks in the list range from 4.7% to 0.7%, and the proposed DIFL-FR error is 0.61%, which is the best result of the two/three-layer models.

2) Fashion-MNIST Dataset

In this section, the proposed method DIFL-FR is evaluated on the Fashion-MNIST image dataset. The Fashion-MNIST image dataset is an alternative image dataset of the MNIST dataset. The dataset consists of 70,000 images of different items in 10 categories (T-shirts, trousers, pullovers, skirts, sneakers, etc.). The size, format, and training set/test set partitioning of the Fashion-MNIST dataset are identical to those of the MNIST dataset.

TABLE V
COMPARISON OF ACCURACY ON THE MNIST DATASET FOR EACH METHOD (%)

Traditional Method	Raw	BlockHist	LBP	PCA	KPCA	Fisherface
Accuracy	92.9	91.07	94.68	91.79	—	85.37
Deep Learning Method	CNN(6-2-16-2)	LeNet-5[25]	DBM[40]	StrongNet[41]	DIFL-FR	
Accuracy	98.8	99.05	99.05	98.9	99.39	

Note: In the comparative experiment, KPCA has no experimental result because the latitude of the construction kernel matrix is too large and exceeds the memory. The experimental results of Lenet-5, DBM and StrongNet are quoted from the results of [25],[40],[41] respectively.

TABLE VI
COMPARISON OF ACCURACY ON THE FASHION-MNIST DATASET FOR EACH METHOD (%)

Traditional Method	Raw	BlockHist	LBP	PCA	KPCA	Fisherface
Accuracy	84.1	81.18	82.19	83.93	—	79.56
Deep Learning Method	CNN(6-2-16-2)	DNN		VGG 16	DIFL-FR	
Accuracy	89.24	88.33		93.5	91.77	

Note: In the comparison experiment, KPCA has no experimental result because the latitude of the construction kernel matrix is too large and exceeds the memory.

Similarly, on the Fashion-MNIST dataset, in addition to the same aforementioned comparative algorithms, a DNN with three hidden layers was also evaluated where the hidden layer structure is 256-128-100. We select the mean square error as the loss function, the tanh function as the activation function, and the SGD as the optimization algorithm; the number of epochs is set as 100. In addition, a CNN framework with more layers, the VGG 16 network, is compared. In the experiment, the standard VGG 16 structure is adopted, where the cross-entropy loss, ReLU activation function and Adam optimization algorithm are adopted, and the number of epochs is set as 100. Table VI shows the accuracies of these methods. The DIFL-FR is superior to the traditional feature extraction methods and the two/three-layer neural networks but slightly inferior to the VGG 16 model. However, the proposed method is more interpretable than the VGG 16 model due to the introduction of rules in it. Moreover, the performance of the proposed method can be further enhanced when an improved criterion, such as a semi-supervised objective, is adopted to learn the parameters of the fuzzy rules.

For the effectiveness analysis of the DIFL-FR fuzzy system feature extraction module, please see Part F of the *Supplementary Materials* section. Moreover, a more comprehensive parameter analysis of the proposed DIFL-FR method is also presented in Part G of the *Supplementary Materials* section.

V. CONCLUSIONS

The paper proposes a deep image feature learning method with fuzzy rules, which is based on the TSK-FS stacked feature learning structure. The experimental results show that the proposed method is superior to the traditional hand-crafted feature extraction method. Compared with DNNs, which tend to overfit when there are too few samples in the training sets, the proposed method achieves satisfactory results on small datasets. On the larger-scale datasets, the results of the proposed method are comparable to those of the deep neural networks. In particular, the feature learning with fuzzy rules in DIFL-FR not only provides nonlinear feature learning to enhance the learning ability but also offers good interpretability.

In the future, we will conduct in-depth research into deep image feature learning based on TSK-FS from the following aspects. In the proposed DIFL-FR, the depth of the network structure will be explored to further increase the capacity of the model. Furthermore, this paper uses a PCA to preserve the geometric properties of the data in the feature learning phase of each layer, which can only preserve the global structure of the data under unsupervised learning. In future studies, we will attempt to use techniques that can preserve the local structure of the data and add supervised learning strategies to further improve the performance.

REFERENCES

- [1] N. Dalal and B. Triggs, "Histograms of Oriented Gradients for Human Detection," in *2005 IEEE Computer Society Conference on Computer Vision and Pattern Recognition (CVPR'05)*, San Diego, CA, USA, Jun. 2005, pp. 886–893.
- [2] T. Ojala, M. Pietikainen, and T. Maenpaa, "Multiresolution gray-scale and rotation invariant texture classification with local binary patterns," *IEEE transactions on Pattern Anal. Machine Intell.*, vol. 24, no. 7, pp. 971–987, 2002.
- [3] F.-F. Li and P. Perona, "A Bayesian Hierarchical Model for Learning Natural Scene Categories," in *2005 IEEE Computer Society Conference on Computer Vision and Pattern Recognition (CVPR'05)*, San Diego, CA, USA, Jun. 2005, pp. 524–531.
- [4] L. Liu, L. Wang, and X. Liu, "In defense of soft-assignment coding," in *2011 International Conference on Computer Vision, Barcelona*, Spain, Nov. 2011 - Nov. 2011, pp. 2486–2493.
- [5] J. Philbin, O. Chum, M. Isard, J. Sivic, and A. Zisserman, "Lost in quantization: Improving particular object retrieval in large scale image databases," in *2008 IEEE Conference on Computer Vision and Pattern Recognition*, Anchorage, AK, USA, Jun. 2008 - Jun. 2008, pp. 1–8.
- [6] J. Wang et al., "Locality-constrained Linear Coding for image classification," in *2010 IEEE Computer Society Conference on Computer Vision and Pattern Recognition*, San Francisco, CA, USA, Jun. 2010 - Jun. 2010, pp. 3360–3367.
- [7] J. Yang, K. Yu, Y. Gong, and T. Huang, "Linear spatial pyramid matching using sparse coding for image classification," in *2009 IEEE Conference on Computer Vision and Pattern Recognition*, Miami, FL, Jun. 2009 - Jun. 2009, pp. 1794–1801.
- [8] A. Gersho and B. Ramamurthi, "Image coding using vector quantization," in *ICASSP '82. IEEE International Conference on Acoustics, Speech, and Signal Processing*, Paris, France, May.

- 1982, pp. 428–431.
- [9] G. J. Garateguy, G. R. Arce, D. L. Lau, and O. P. Villarreal, “QR images: optimized image embedding in QR codes,” *IEEE transactions on image processing*, vol. 23, no. 7, pp. 2842–2853, 2014.
- [10] Q. Zhang and B. Li, “Discriminative K-SVD for dictionary learning in face recognition,” in *2010 IEEE Computer Society Conference on Computer Vision and Pattern Recognition*, San Francisco, CA, USA, Jun. 2010 - Jun. 2010, pp. 2691–2698.
- [11] J. Yang, J. Wright, T. S. Huang, and Y. Ma, “Image super-resolution via sparse representation,” *IEEE transactions on image processing*, vol. 19, no. 11, pp. 2861–2873, 2010.
- [12] M. Turk and A. Pentland, “Eigenfaces for recognition,” *Journal of Cognitive Neuroscience*, vol. 3, no. 1, pp. 71–86, 1991.
- [13] S. Wold, K. Esbensen, and P. Geladi, “Principal component analysis,” *Chemometrics and Intelligent Laboratory Systems*, vol. 2, no. 1-3, pp. 37–52, 1987.
- [14] P. N. Belhumeur, J. P. Hespanha, and D. J. Kriegman, “Eigenfaces vs. Fisherfaces: Recognition using class specific linear projection,” in *Lecture Notes in Computer Science, Computer Vision — ECCV ’96*, G. Goos, J. Hartmanis, J. van Leeuwen, B. Buxton, and R. Cipolla, Eds., Berlin, Heidelberg: Springer Berlin Heidelberg, 1996, pp. 43–58.
- [15] J. Lu, K. N. Plataniotis, and A. N. Venetsanopoulos, “Face recognition using LDA-based algorithms,” *IEEE transactions on neural networks*, vol. 14, no. 1, pp. 195–200, 2003.
- [16] Y. Bengio and O. Delalleau, “On the Expressive Power of Deep Architectures,” in *Lecture Notes in Computer Science, Algorithmic Learning Theory*, J. Kivinen, C. Szepesvári, E. Ukkonen, and T. Zeugmann, Eds., Berlin, Heidelberg: Springer Berlin Heidelberg, 2011, pp. 18–36.
- [17] G. E. Hinton, S. Osindero, and Y.-W. Teh, “A fast learning algorithm for deep belief nets,” *Neural computation*, vol. 18, no. 7, pp. 1527–1554, 2006.
- [18] A. Krizhevsky, I. Sutskever, and G. E. Hinton, “ImageNet classification with deep convolutional neural networks,” *Commun. ACM*, vol. 60, no. 6, pp. 84–90, 2017.
- [19] Y. Bengio, A. Courville, and P. Vincent, “Representation learning: a review and new perspectives,” *IEEE transactions on Pattern Anal. Machine Intell.*, vol. 35, no. 8, pp. 1798–1828, 2013.
- [20] Hecht-Nielsen, “Theory of the backpropagation neural network,” in *International Joint Conference on Neural Networks, Washington, DC, USA, Jun. 1990 - Jun. 1990*, 593-605 vol.1.
- [21] L. Bottou, “Large-Scale Machine Learning with Stochastic Gradient Descent,” in *Proceedings of COMPSTAT’2010*, Y. Lechevallier and G. Saporta, Eds., Heidelberg: Physica-Verlag HD, 2010, pp. 177–186.
- [22] R. Alcalá, J. Alcalá-Fdez, J. Casillas, O. Cordón, and F. Herrera, “Local identification of prototypes for genetic learning of accurate TSK fuzzy rule-based systems,” *Int. J. Intell. Syst.*, vol. 22, no. 9, pp. 909–941, 2007.
- [23] Y. Zhang, H. Ishibuchi, and S. Wang, “Deep Takagi–Sugeno–Kang fuzzy classifier with shared linguistic fuzzy rules,” *IEEE Trans. Fuzzy Syst.*, vol. 26, no. 3, pp. 1535–1549, 2018.
- [24] P.-C. Chang and C.-H. Liu, “A TSK type fuzzy rule based system for stock price prediction,” *Expert Systems with Applications*, vol. 34, no. 1, pp. 135–144, 2008.
- [25] Y. Lecun, L. Bottou, Y. Bengio, and P. Haffner, “Gradient-based learning applied to document recognition,” *Proc. IEEE*, vol. 86, no. 11, pp. 2278–2324, 1998.
- [26] C. Szegedy et al., “Going deeper with convolutions,” in *2015 IEEE Conference on Computer Vision and Pattern Recognition (CVPR)*, Boston, MA, USA, Jun. 2015 - Jun. 2015, pp. 1–9.
- [27] K. Simonyan and A. Zisserman, “Very Deep Convolutional Networks for Large-Scale Image Recognition,” *Computer Science*, 2014.
- [28] B. Zhou, A. Khosla, A. Lapedriza, A. Oliva, and A. Torralba, “Learning Deep Features for Discriminative Localization,” in *2016 IEEE Conference on Computer Vision and Pattern Recognition (CVPR)*, Las Vegas, NV, USA, Jun. 2016 - Jun. 2016, pp. 2921–2929.
- [29] T. Takagi and M. Sugeno, “Fuzzy identification of systems and its applications to modeling and control,” *IEEE transactions on Syst., Man, Cybern.*, vol. SMC-15, no. 1, pp. 116–132, 1985.
- [30] H. Carter, D. Dubois, and H. Prade, “Fuzzy Sets and Systems -- Theory and Applications,” *The Journal of the Operational Research Society*, vol. 33, no. 2, p. 198, 1982.
- [31] M. Sugeno and G.T. Kang, “Structure identification of fuzzy model,” *Fuzzy Sets and Systems*, vol. 28, no. 1, pp. 15–33, 1988.
- [32] J. C. Bezdek, *Pattern Recognition with Fuzzy Objective Function Algorithms*. Boston, MA: Springer US, 1981.
- [33] A. Blum and T. Mitchell, “Combining labeled and unlabeled data with co-training,” in *Proceedings of the eleventh annual conference on Computational learning theory - COLT’ 98*, Madison, Wisconsin, United States, 1998, pp. 92–100.
- [34] T. Su and J. G. Dy, “In search of deterministic methods for initializing K-means and Gaussian mixture clustering,” *Intelligent Data Analysis*, vol. 11, no. 4, pp. 319–338, 2006.
- [35] C.-C. Chang and C.-J. Lin, “LIBSVM,” *ACM transactions on Intell. Syst. Technol.*, vol. 2, no. 3, pp. 1–27, 2011.
- [36] D. Cai, X. He, J. Han, and H.-J. Zhang, “Orthogonal Laplacianfaces for Face Recognition,” *IEEE transactions on Image Process.*, vol. 15, no. 11, pp. 3608–3614, 2006.
- [37] D. Cai, X. He, and J. Han, “Spectral Regression for Efficient Regularized Subspace Learning,” in *2007 IEEE 11th International Conference on Computer Vision*, Rio de Janeiro, Brazil, Oct. 2007 - Oct. 2007, pp. 1–8.
- [38] X. He, S. Yan, Y. Hu, P. Niyogi, and H.-J. Zhang, “Face recognition using laplacianfaces,” *IEEE transactions on Pattern Anal. Machine Intell.*, vol. 27, no. 3, pp. 328–340, 2005.
- [39] H. Xiao, K. Rasul, and R. Vollgraf, “Fashion-MNIST: a Novel Image Dataset for Benchmarking Machine Learning Algorithms,” 2017.
- [40] R. Salakhutdinov and G. Hinton, “An efficient learning procedure for deep Boltzmann machines,” *Neural computation*, vol. 24, no. 8, pp. 1967–2006, 2012.
- [41] M. Albonico et al., “StrongNet: An International Network to Improve Diagnostics and Access to Treatment for Strongyloidiasis Control,” *Plos Neglected Tropical Diseases*, vol. 10, no. 9, e0004898, 2016.